NOTES AND CORRESPONDENCE

Estimates of Surface and Subsurface Forcing for Decadal Sea Surface Temperature Variability in the Mid-Latitude North Pacific

Tomohiko TOMITA

Frontier Research System for Global Change, Institute for Global Change Research, Yokohama, Japan

Shang-Ping XIE

International Pacific Research Center, School of Ocean and Earth Science and Technology, University of Hawaii at Manoa, HI, USA
Department of Meteorology, University of Hawaii at Manoa, HI, USA

and

Masami NONAKA

Frontier Research System for Global Change, Institute for Global Change Research, Yokohama, Japan
International Pacific Research Center, School of Ocean and Earth Science and Technology, University of Hawaii at Manoa, HI, USA

(Manuscript received 18 December 2001, in revised form 2 July 2002)

Abstract

The upper ocean, atmosphere and their interaction over the North Pacific exhibit pronounced decadal to interdecadal variations. A diagnostic equation for analyzing the heat budget for decadal variability in winter sea surface temperature (SST) is derived that can properly account for subsurface geostrophic advection, and strong seasonal cycle in the depth and temperature of the ocean mixed layer. A model-assimilated ocean dataset, partially validated for the period of the TOPEX/Poseidon mission, is used to evaluate the relative importance of subsurface advection and surface forcing due to wind-induced turbulent heat flux and Ekman advection. For our analysis, two key regions are chosen where decadal SST variance reaches local maxima, centered at 170°E, 42°N (Region A) and 155°W, 35°N (Region B), respectively.

Region B is under the direct influence of the Aleutian Low, where the surface effects are dominant. Region A is part of the Kuroshio-Oyashio Extension, where the winter mixed layer is deep and the subsurface geostrophic advection contributes significantly to low-frequency winter SST variations. Our analysis suggests that anomalous geostrophic advection changes signs north and south 38°N, presumably as a result of ocean gyre circulation adjustment to wind changes to the east. The surface forcing shows a larger-scale structure covering the entire mid-latitude North Pacific, in response to basin-wide changes in atmospheric circulation.

Corresponding author and present affiliation: Tomohiko Tomita, Department of Environmental Sciences, Faculty of Science, Kumamoto University, Kumamoto 860-8555, Japan.
E-mail: tomita@sci.kumamoto-u.ac.jp

1. Introduction

Low-frequency variations on interdecadal timescales are observed in winter sea surface temperature (SST) in the mid-latitude North Pacific (Tanimoto et al. 1993; Deser et al. 1996;

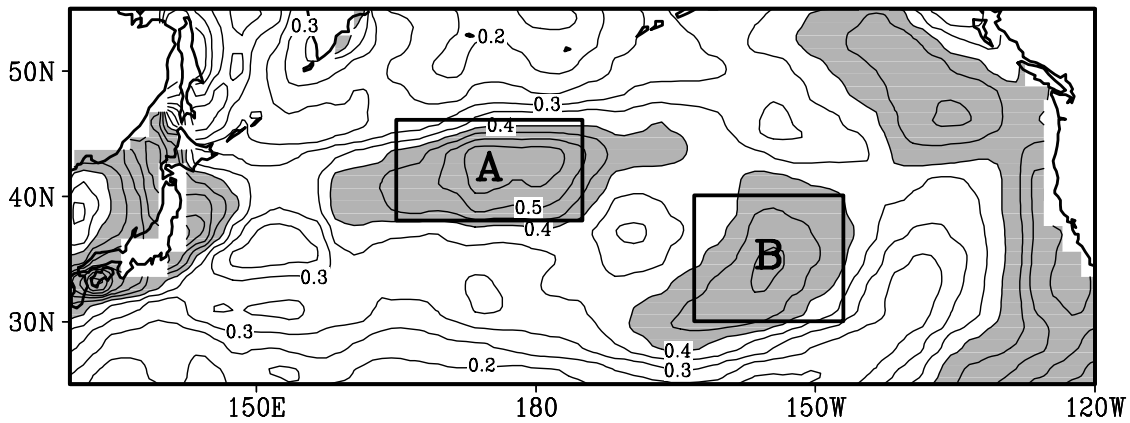

Fig. 1. Rms variance in °C of low-pass filtered (>5 yr) SST in winter (January–March) in the mid-latitude North Pacific. Contour intervals are 0.05°C, with values greater than 0.4°C shaded. Key regions to be analyzed, namely Regions A (165°E–175°W, 38°–46°N) and B (163°–147°W, 30°–40°N), are marked by boxes.

Nakamura et al. 1997; Tomita et al. 2001). The centers of action, defined here by large root-mean-square (rms) variance of low-pass filtered winter SST anomalies (SSTAs), appear along the sub-arctic frontal zone near the dateline and to the southeast (Fig. 1).

Wind-induced changes in surface heat flux are a major forcing for non-seasonal SST variation in the off-equatorial oceans (Frankignoul 1985; Cayan 1992). Positive (negative) SSTAs are often found to be associated with a weakening (enhancement) of the prevailing wind. In the tropics, this local wind-SST co-variability leads to a wind-evaporation-SST feedback that favors a distinctive spatial pattern anti-symmetric about the equator (Xie et al. 1999). In the extratropics, however, such coherence between local wind and SST is either interpreted as evidence in support of the stochastic forcing scenario (Frankignoul 1985) or attributed to tropical forcing such as El Niño/Southern Oscillation (ENSO; Alexander et al. 2002).

Subsurface ocean dynamics have been suggested as important for low-frequency SST variations in the North Pacific (Latif and Barnett 1994). Indeed, a recent study based on an ocean general circulation model (GCM) hindcast (Xie et al. 2000) identified the Kuroshio-Oyashio Extension (KOE) region east of Japan as a window of coupling between SST and subsurface ocean that opens only in winter (see also Miller et al. 1994; Schneider et al. 2002). This is consistent with Qiu (2000) who found that geostrophic advection estimated from satellite altimetry measurements was much larger than Ekman advection and comparable with surface heat flux forcing in the Kuroshio Extension (141°E–180, 31°–37°N; see also Qiu and Kelly (1993), Yasuda et al. (2000)). Because of lack of in-situ observations over the vast North Pacific, direct estimates of subsurface advective effect on low-frequency SST variability have not been possible. Qiu (2000) is an exception, but the use of TOPEX/Poseidon (T/P) altimetry limited his analysis to a short period for 1992–99.

The present study is an attempt at a direct estimate of geostrophic advection to assess its relative importance to local surface processes of surface turbulence heat flux and Ekman advection. The in-situ observations are too sparse, while satellite altimetry measurements are too short duration to address decadal variability. Here, we use a new model-assimilated dataset called the Simple Ocean Data Assimilation (SODA; Giese and Carton 1999; Carton et al. 2000), which assimilates nearly all the available surface and subsurface measurements, in-situ and by satellite, and uses an ocean GCM to interpolate these data of various types. Such

model-assimilated datasets will certainly improve as the assimilation techniques improve and more data are collected. We consider it a useful exercise to evaluate the advective effect using the currently available SODA, given that it has never been done before for decadal variability. Indeed, we will show that advection anomalies from SODA and T/P generally agree during their overlapping period.

The second purpose of this study is to devise a methodology for subsurface advection estimate. Previously, some authors estimated the advection only during the winter season (Miller et al. 1994; Yasuda and Hanawa 1997; Qiu 2000), but subsurface ocean temperature is known to carry the history of previous winters (Alexander et al. 1999). It is unclear how to estimate the turbulent entrainment heat flux that is strong at the mixed layer bottom during boreal fall. We will propose a diagnostic scheme that effectively sidesteps this difficulty with turbulent mixing. The two SSTA centers of action in the central North Pacific and to its east (Fig. 1) are the focus of this study. We will apply this scheme and estimate the subsurface advection.

In the rest of this note, Section 2 introduces datasets to be used. Section 3 derives a tendency equation for the ocean mixed-layer temperature. Section 4 applies this tendency equation to the assimilation data and evaluates the effects of surface and subsurface variations on decadal SSTAs. Section 5 gives a summary of this work.

2. Data

We use the following four datasets. The first is the SODA, which is based on multivariate optimal interpolation using the Modular Ocean Model-2 physics (Carton et al. 2000). The SODA analysis provides three-dimensional fields of salinity, temperature, and current velocity in the global ocean from 60°S to 60°N for the period 1950–99 at monthly time resolution. The spatial resolution is approximately 1° in both longitudinal and latitudinal directions. In the vertical, there are 20 levels with a resolution of 15 m near the surface. The number of subsurface observations below 250 m increased dramatically in the late 1960s as a result of the use of expendable bathythermograph (XBT) and conductivity-temperature-depth (CTD) sensors. The spatial density of observations is high in the mid-latitude North Pacific because of major shipping lanes between Asia, Hawaii, and North America (see Fig. 1 of Carton et al. 2000). The present work, therefore, sets the analysis domain to the mid-latitude North Pacific and the analysis period from 1970 to 1999. A quality check of SODA is performed in Fig. 2 that shows the long-term (1970–99) mean mixed layer in winter. Since salinity contributes to the formation of mixed layer in mid-

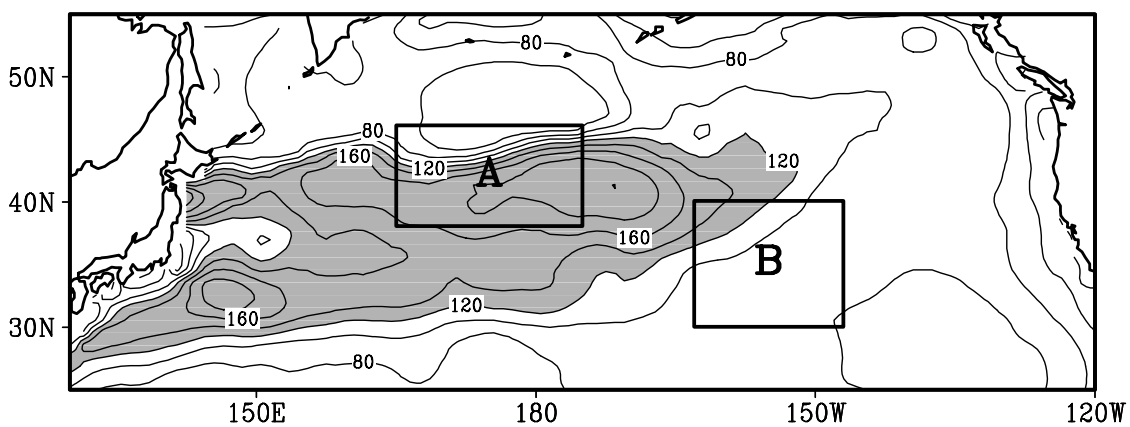

Fig. 2. Long-term (1970–99) mean of winter (January–March) mixed layer depth. Contour interval is 20 m, with values deeper than 120 m shaded.

and high-latitudes, the mixed layer is defined as where the density is within 0.125 kg m^{-3} of the surface value. It is confirmed that the mixed layer distribution based on SODA is similar to observations (cf., Huang and Qiu 1994).

The second is the global ice and SST (GISST) dataset compiled at the U. K. Meteorological Office, which is provided on a $1^\circ \times 1^\circ$ lon.-lat. grid for the period of 1903–99 (Rayner et al. 1996). The missing data without sufficient observations are reconstructed by a linear sum of covariance empirical orthogonal functions weighted by corresponding adjusted time coefficients (Parker et al. 1995). For the 30-year period we focus on here, the data quality is generally good over the North Pacific.

The SODA version we analyzed does not provide the atmospheric thermal forcing applied to the model. We use the National Centers for Environmental Prediction/National Center for Atmospheric Research (NCEP/NCAR) reanalysis (Kalnay et al. 1996) for surface thermal forcing estimation. The surface variables are available at monthly time resolution from 1948 to 1999, covering the entire globe on the Gaussian grid.

The altimeters on the T/P and European Remote Sensing (ERS) satellites provide observations of sea surface height since 1992. To validate the geostrophic advection estimated from the SODA analysis data, we employ the observations complied to those at monthly time resolution from 1992 to 1999 and on a $1^\circ \times 1^\circ$ lon.-lat. grid in the Pacific with GISST.

To filter out the interannual signals of ENSO and to highlight the lower-frequency variations, we apply the 5-term weighted running mean to yearly time series throughout this work, in which the weights are derived from the binomial coefficients, namely (1, 4, 6, 4, 1)/16. Using autocorrelation function (Fraedrich et al. 1995), the degree of freedom of the smoothed time series is estimated for the Student t-test of significance.

3. Winter mixed-layer heat budget

The method of diagnosing the budget of winter SST variations is not well established. Some studies focus exclusively on the winter-mean contributions by ocean-atmospheric processes (Miller et al. 1994; Yasuda and Hanawa 1997; Qiu 2000), which may underestimate the ocean dynamic effects as shown in Subsection 3.2. Here, we develop a diagnostic scheme for mixed layer heat budget.

3.1 Tendency equation

The governing equation for ocean temperature T is

$$\frac{\partial T}{\partial t} = -\mathbf{u}\cdot\nabla T - w\frac{\partial T}{\partial z} + \frac{\partial}{\partial z}\left(\kappa\frac{\partial T}{\partial z}\right), \tag{3.1}$$

where $\mathbf{u}$ and w are the horizontal and vertical velocities, respectively, and κ is the eddy diffusivity. Here we have neglected the horizontal diffusion term. Integrating this equation from the surface to the maximum depth of winter mixed layer (h) gives rise to

$$\frac{\partial}{\partial t}\int_0^h T\,dz = -\int_0^h \mathbf{u}\cdot\nabla T\,dz + \frac{Q}{c_p\rho} - Vert, \tag{3.2}$$

where Q is surface heat flux, c_p and ρ are the specific heat at constant pressure and density of seawater, and *Vert* combines the advective and diffusive flux at $z = h$. In the mid-latitude North Pacific, the mixed layer is deepest and SSTs are at the minimum in March. Integrating (3.2) for one year from March of year $(n-1)$ to March of year n yields

$$\frac{\Delta T_{mw}}{\Delta t} = -\underbrace{\langle \mathbf{U}_E\cdot\nabla T_m\rangle/h}_{E} - \underbrace{\frac{1}{h}\int_0^h \langle \mathbf{u}_g\cdot\nabla T\rangle\,dz}_{G} + \frac{\langle Q\rangle}{c_p\rho h} - \langle Vert\rangle/h, \tag{3.3}$$

where the subscript m denotes the values in the mixed layer, w winter values, g and E geostrophic and Ekman components of the ocean current. The bracket denotes the annual average: $\langle\ \rangle = \frac{1}{\Delta t}\int_0^{\Delta t} dt$; Δt denotes the difference between two consecutive Marches ($\Delta t = 1$ year); and $\mathbf{U}_E = \boldsymbol{\tau}\times\boldsymbol{k}/(\rho f)$ is the Ekman transport where $\boldsymbol{\tau}$ is the surface wind stress, $\boldsymbol{k}$ and f are the vertical unit vector and the Coriolis parameter. Thus, E and G are the advection by the Ekman and geostrophic flow, respectively.

If the March SST does not change interannually, the right hand side (rhs) of Eq. (3.3) reaches a balance. Defining interannual anomalies as $E' = E - \bar{E}$ with the overbar denoting the long-term mean, we obtain a ten-

dency equation for low-frequency variations in March SST

$$\frac{\Delta T_{mw}}{\Delta t} = -E' - G' + \langle Q \rangle' / c_p \rho h - \langle Vert \rangle' / h. \tag{3.4}$$

Section 4 makes a quantitative estimate of each term on the rhs. We will neglect the vertical flux at $z = h$ because the vertical advection is small in the mid-latitudes and the turbulent entrainment at the bottom of the winter mixed layer is small (e.g., Qiu 2000). The seasonal entrainment associated with the deepening mixed layer from fall to winter and its interannual variations are implicitly included in our formulation as discussed below.

3.2 Geostrophic advection

Equation (3.4) states that the rate of change of low-frequency winter SST is caused by the annual-means of advection and heat flux instead of the winter means. Why do winter SST anomalies care about geostrophic advection in summer? To illustrate this, let us assume that the seasonal deepening of the mixed layer takes place abruptly at the end of summer, $t = t_{n-1/2}$ (Fig. 3). The associated entrainment resets the mixed layer temperature to the vertical mean temperature within the winter mixed layer as geostrophic advection keeps changing subsurface temperature in summer (Schneider et al. 2002). Therefore, a heat budget analysis using only three-month winter data will underestimate the geostrophic advection by a factor of four (geostrophic currents have only a weak seasonal cycle in the mid-latitudes).

If one only focuses the heat budget near the sea surface (say at the first vertical grid point), he may find a large contribution by the entrainment in late fall and early winter. But this apparent entrainment of subsurface anomalies ultimately comes from geostrophic advection during the warm seasons. In the late winter, the entrainment is weak as the mixed layer reaches its maximum depth.

In the absence of horizontal advection ($E' = 0$ and $G' = 0$), Eq. (3.4) is reduced to that describing the local re-emergence mechanism, in which winter deep mixing entrains water temperature set in the previous winter (Alexander et al. 1999). Thus, our formulation may be viewed as a generalization of the local re-emergence mechanism that includes non-local advective effects.

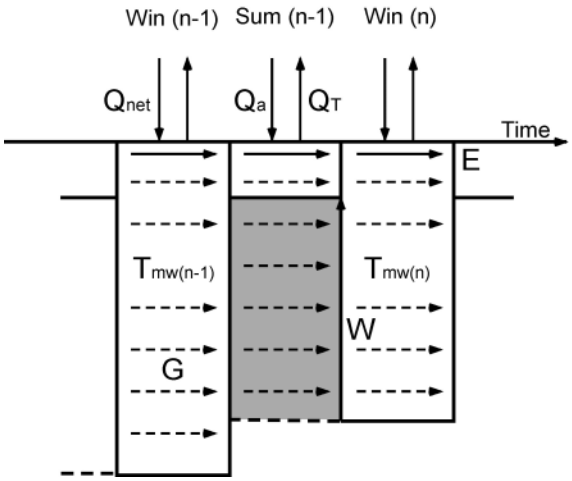

Fig. 3. Schematic diagram of seasonal variations in the mixed layer. $Q_{\rm net}$, Q_a, and Q_T are for surface heat flux. E, G, and W signify Ekman and geostrophic advections, and vertical entrainment, respectively. $T_{mw(n)}$ indicates winter mixed layer temperature in an arbitrary year n. Shade implies the summer sub-mixed layer where seawater is entrained in winter.

3.3 Decomposition of surface heat flux

While latent heat flux Q_E is often treated as a single term, it contains two physically distinct components: atmospheric forcing and oceanic response. Anomalous wind-induced flux change is just one example of the former that is a key to air-sea interaction in the off-equatorial tropics (Xie et al. 1999). The latter arises from the temperature dependence of evaporation and can be sometimes linearized as a Newtonian cooling (Haney 1971). In the mid-latitudes where temperature gradient is large and winds are strong, advective effects on air temperature and humidity are not negligible. Because such advective effects are difficult to quantify, we will decompose latent and sensible heat (Q_H) flux into wind-induced component

$$Q'_a = \frac{-W'}{\overline{W}} (\overline{Q}_E + \overline{Q}_H), \tag{3.5}$$

and the residual Q'_T

$$Q'_E + Q'_H = Q'_a + Q'_T, \tag{3.6}$$

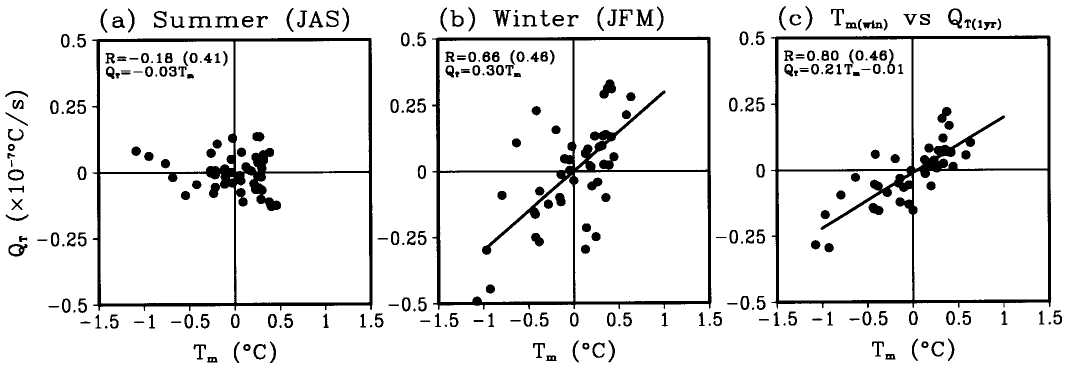

Fig. 4. Scatter diagrams of winter mixed-layer temperature (T_m) and seasonal-mean Q_T over the northern mid-latitude North Pacific (160°E–160°W, 38°–45°N), (a) in summer (July–September) and (b) in winter (January–March). (c) is same as (a) and (b) but for T_m and annual-mean Q_T. The correlation coefficient (R) and the regression relation between Q_T and T_m are displayed at the upper-left part in each panel. The number in parentheses for R is the correlation coefficient at the 95% level based on the two-tailed Student t-test.

where W is the wind speed. Although Q'_T also includes atmospheric advective effects, it is indeed highly correlated with SST anomalies (Fig. 4). Thus, we can approximate it as a linear Newtonian damping, $Q'_T \approx \varepsilon T'_m$. For low-frequency SST variations caused by wind-induced heat flux changes (frequency $\omega \ll \varepsilon \sim (1\ \text{year})^{-1}$), the forcing ($Q'_a$) and response ($Q'_T$) can be largely in balance. As a result, the net heat flux vanishes. Diagnosis based on the net heat flux would conclude, incorrectly, that heat flux forcing is unimportant.

In summer, Q'_T and winter mixed-layer temperature (T'_m) are not correlated (Fig. 4a). Because of this and because the winter SSTAs tend to be larger than the summer ones in most of the mid-latitude North Pacific, $\langle Q'_T \rangle$ is determined by the Newtonian cooling in winter. Indeed, the correlation between $\langle Q'_T \rangle$ and winter mixed layer temperature is very high (0.80, Fig. 4c). An effective damping rate can be estimated from Fig. 4c: $\varepsilon^* = (1.5\ \text{year})^{-1}$, suggesting that on decadal and longer timescales, the terms on the rhs of Eq. (3.4) are nearly in balance.

In the following analysis, we use the NCEP/NCAR reanalysis for surface heat flux. No attempt is made to estimate the shortwave and longwave radiative flux not because it is unimportant but because of the large uncertainties in it in the reanalysis (Kalnay et al. 1996). The SODA data are used to estimate Ekman and geostrophic advections. Because the atmospheric and oceanic variables are from independent assimilated model results, we do not attempt to close the heat budget. Our estimates would improve if SODA had used the NCEP surface heat flux in the assimilation.

4. Contribution of surface and subsurface effects

Large decadal SST variance reaches local maxima in the following two areas: Region A around the dateline and in the northern KOE (165°E–175°W, 38°–46°N), and Region B in the eastern North Pacific (163°–147°W, 30°–40°N) as marked in Fig. 1 (Miller et al. 1994; Deser et al. 1996; Nakamura et al. 1997; Tomita et al. 2001). In this section, we estimate the geostrophic advection, Ekman advection, and wind-induced heat flux terms at these two centers of action of decadal SST variations in the mid-latitude North Pacific. Since they are both proportional to wind speed changes, we will combine the Ekman advection and wind-induced surface heat terms and call their sum the surface forcing. Figures 5 and 6 illustrate winter (January–March) mean SST variations at the two centers of action, and the corresponding time series of geostrophic advection and surface forcing terms, which are divided by the local damping rate (ε^*) to diagnose the effective forcing in °C. The rms of variance and correlation statistics are summarized in Table 1.

4.1 Box mean

Region A displays quasi-decadal SST variations, with positive maxima in early 1970s, 80s and 90s (Fig. 5a). Subsurface forcing is significantly correlated with SSTA, indicating that it consistently acts to produce low-frequency winter SSTAs in Region A (Table 1). On the other hand, surface forcing also contributes to the low-frequency SST variations, especially in periods such as early 1970s or late 1980s (Fig. 5c).

In Region B, subsurface advection is small in magnitude and is not significantly correlated with SSTA (Fig. 6b and Table 1). In comparison, surface forcing is strong and highly correlated with SSTA (Fig. 6c and Table 1). Thus we conclude that the surface Ekman advection and wind-induced heat flux are the dominant forcing for low-frequency SST variations in Region B. As such, the contribution of subsurface effects toward low-frequency winter SSTAs varies over the mid-latitude North Pacific.

Deser et al. (1996) reported that in the KOE region, the seawater temperature anomalies are in phase from the surface to at least 400-m without much attenuation in amplitude. In the eastern North Pacific, by contrast, temperature anomalies lag in phase and decreases in amplitude with increasing depth. Such differences in

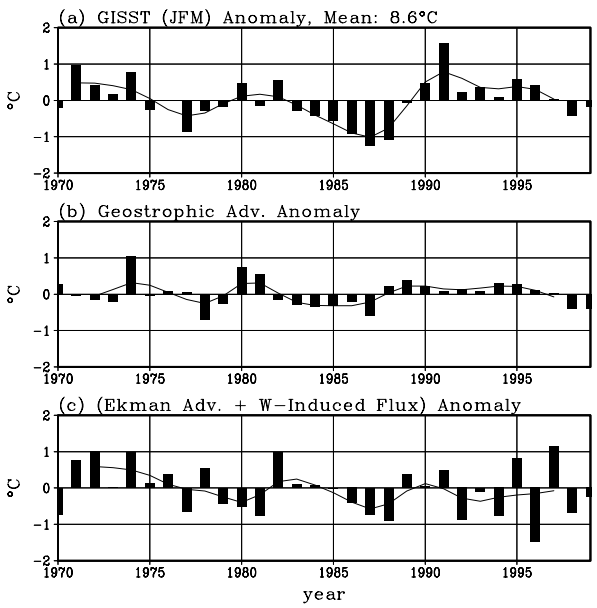

Fig. 5. (a) unsmoothed (bars) and low-pass filtered (solid line) SST anomalies in winter (January–March), anomalies of (b) geostrophic advection and (c) surface forcing (Ekman advection plus wind-induced heat flux), all area-averaged in Region A (Fig. 1). (b) and (c) are annual-averages from April of the preceding year to March. Unit is °C for the three panels.

Table 1. Rms variance in °C of low-pass filtered (>5 yr) winter (January–March) SST, geostrophic advection (GA), and the sum of Ekman advection and wind-induced heat flux (EA+WF) in Regions A and B. The latter two variables are annual mean from April of the preceding year to March. In parentheses are the correlation coefficients with SST, with the bold face denoting correlations significant at the 95% level (0.58) based on a two-tailed Student *t*-test.

	SST(JFM)	GA	EA+WF
Region A	0.47	0.21 (**0.70**)	0.30 (0.39)
Region B	0.42	0.16 (0.55)	0.54 (**0.66**)

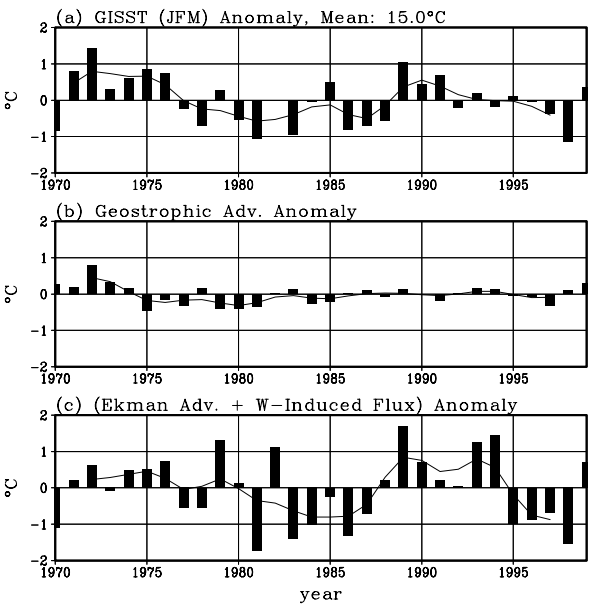

Fig. 6. As in Fig. 5 but for Region B.

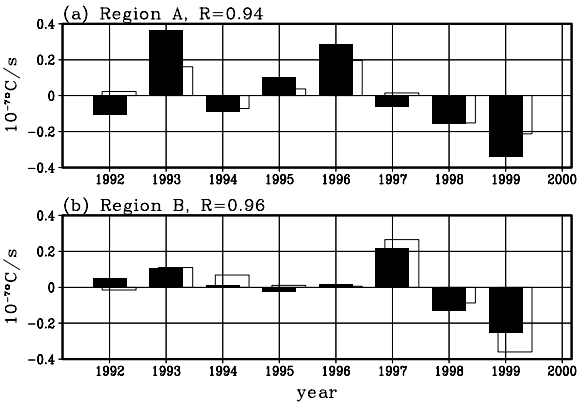

Fig. 7. Annual-mean geostrophic advection anomalies estimated from the SODA analysis data (filled bars) and from the GISST, and T/P and ERS altimetry data (open) as a function of time in Regions A (a) and B (b). Correlations between the two estimates are above 0.9, significant at the 99% level (0.83). The anomalies are defined as the deviations from the 8-year mean for 1992–99.

the vertical structure of temperature anomaly are consistent with our heat budget analysis, suggesting that ocean dynamics are important in the KOE (Region A), while surface forcing is dominant in the eastern North Pacific (Region B).

In order to validate the reliability of geostrophic advection estimated from the SODA data, we compare it with an alternative estimate based on observational data only, namely GISST, and T/P and ERS altimetry data for the period 1992–99 (Fig. 7). The advection by anomalous current velocity, $\mathbf{u}'_g \cdot \nabla T$, is computed by using geostrophic current anomaly ($\mathbf{u}'_g$) derived from monthly satellite sea level height anomaly and SST in winter (T). Here we use T to approximate winter mixed-layer temperature and subsurface temperature beneath the seasonal thermocline in warm seasons. The temporal variability agrees remarkably well between the two estimates and their correlations are above 0.9 and significant at the 99% level in both Regions A and B. The agreement may be partially due to the assimilation of T/P and ERS data in SODA, but their agreement is at least comforting and gives us some confidence in SODA.

4.2 Spatial distribution

In order to diagnose the spatial distribution of surface and subsurface effects, we performed composite analysis using decadal SST variations in Regions A and B as the reference time series, respectively. Figure 8 shows the differences of winter (January–March) SST, geostrophic advection, and the surface forcing between years when SSTAs in Region A are positive and those when they are negative. Corresponding anomalous subsurface currents at 100 m depth (Fig. 8b) and the surface wind anomalies at 10 m (Fig. 8c) are also plotted.

Over the positive SSTA in Region A (Fig. 8a), anomalous geostrophic advection is generally positive in association with north- or northeastward current anomalies (Fig. 8b), but there is considerable scattering in the direction of anomalous current. On the other hand, Fig. 8c shows that the surface wind field is dominated by easterly anomalies in the mid-latitudes, as part of an anti-cyclonic anomalous circulation centered on the Bering Sea. The anomalous easterlies reduce the speed of the prevailing westerly winds and turbulent heat flux from the ocean surface. The combined effects of positive geostrophic advection and reduced surface flux cooling give rise to the maximum warming in Region A. Immediately south of Region A, there is a band of negative anomalies in geostrophic advection while the surface forcing is still positive. In Xie et al.'s (2000) GCM, SST is restored toward the climatology while the full history of observed wind stress is applied. This modeling setting effectively removes anomalous thermal forcing from the atmosphere. In their model, SST anomalies in Region A tend to show opposite polarities to those to the south (not shown), consistent with the north-south dipole structure in the diagnosed geostrophic advection field in Fig. 8b in and south of Region A (see also Miller et al. 1998).

When the low-pass filtered SSTAs are positive in Region B (Fig. 9a), surface forcing is strong and positive due to the anomalous easterlies that weaken the prevailing westerlies (Fig. 9c). The wind anomalies are part of an anti-cyclonic circulation with a center southeast of that in the Region A composite. The

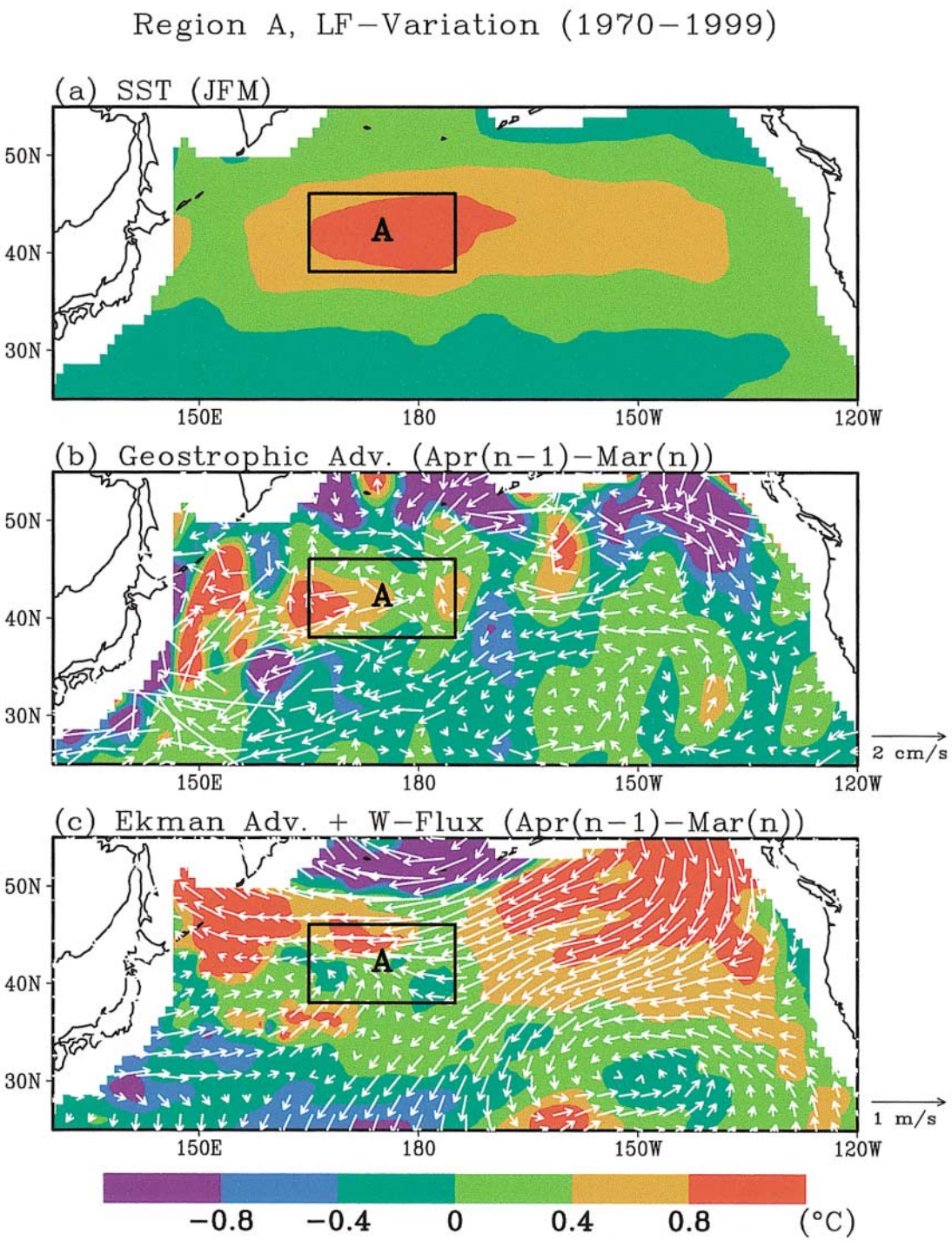

Fig. 8. Composite anomalies based on the SST time series in Region A: (a) SST in winter (January–March), (b) geostrophic advection, and (c) the sum of Ekman advection and wind-induced heat flux. Unit is °C, with the color scale at the bottom. Vectors indicate the anomalous currents at the 100-m depth in (b) and the 10-m height wind anomalies in (c), with the scales shown near each right-bottom corner.

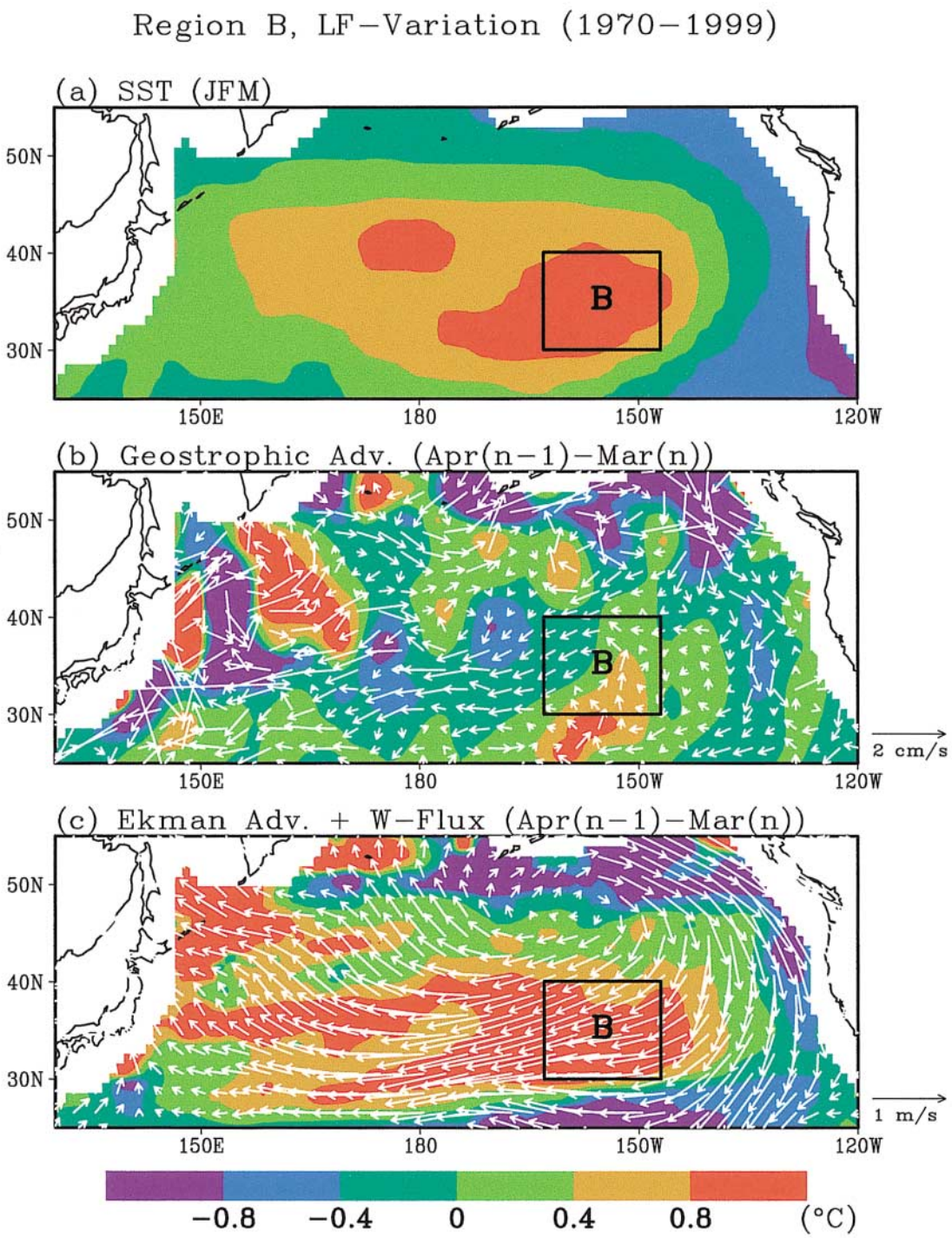

Fig. 9. As in Fig. 8 but for Region B.

geostrophic advection anomalies change sign within Region B (Fig. 9b), making it unlikely to be the major contributor to the SST variability there.

5. Summary

We have derived a diagnostic equation for estimating local surface forcing and subsur-

face dynamic effects on winter-time SSTAs. Our analysis indicates that subsurface geostrophic advection throughout the year contributes to the winter SST, since sub-mixed layer temperature changes during the warm season are entrained into the winter mixed layer by the intense vertical mixing in late fall and winter. Yet, this scheme sidesteps the difficulty of evaluating turbulent mixing by computing the heat budget vertically integrated from the surface to the bottom of the March mixed layer. This diagnostic scheme is a generalization of the local re-emergence mechanism as geostrophic advection causes the temperature beneath the seasonal thermocline to vary slowly during the warm season. Unlike many previous studies, we separate anomalous turbulence surface heat flux into wind-induced forcing and the residual, and show that to a large extent, the residual behaves like a Newtonian cooling and can be treated as a passive oceanic response.

We then use this scheme to diagnose the relative importance of subsurface advection and local surface forcing (wind-induced surface heat flux plus the Ekman advection) in regions of the large decadal SST variance: Region A in the northern KOE (170°E, 42°N) and Region B in the eastern North Pacific (155°W, 35°N). The heat budgets are quite different between them. In Region A, the subsurface advection consistently contributes to decadal winter SSTAs. In Region B, on the other hand, the surface effect dominates while the subsurface advection is very small.

In the KOE region east of Japan, the winter mixed layer is deep (Fig. 2), allowing a significant effect of subsurface advection on SST. Our analysis of geostrophic advection suggests a meridional dipole straddling the 38°N latitude in the western half of the North Pacific (Fig. 8b), presumably a result of the adjustment of ocean gyre circulation to wind changes to the east, which was found in both observations (Deser et al. 1999) and GCM simulations (Miller et al. 1998; Seager et al. 2001). The surface forcing, on the other hand, shows a larger-scale structure extending over the entire mid-latitude North Pacific. As a result, there is a tendency for the surface forcing and subsurface advection to be in-phase north of 38°N and out-of-phase to the south. Such local differences in the surface and subsurface effects are due to the spatial-scale difference between anomalous oceanic and atmospheric circulations.

Our analysis differs from previous modeling studies, in an attempt at a direct estimate of ocean dynamics effect on decadal SSTAs in winter from the model-assimilated SODA. We show that the estimate from SODA agrees with that from T/P and ERS satellite measurements. Along with recent studies (Miller et al. 1994; Deser et al. 1999), our analysis shows that ocean dynamics have a significant role to play in decadal climate variability in the KOE region. How SSTAs there feedback onto the atmosphere is a subject under intense debate and current active research (Peng et al. 1997; Yulaeva et al. 2001).

Acknowledgements

This work is supported by the Institute for Global Change Research of the Frontier Research System for Global Change and NASA grant 49976004. This is the School of Ocean and Earth Science Technology (SOEST) contribution 6016 and the International Pacific Research Center (IPRC) contribution 170.

References

Alexander, M.A., C. Deser, and M.S. Timlin, 1999: The reemergence of SST Anomalies in the North Pacific Ocean. *J. Climate*, **12**, 2419–2433.

———, I. Blade, M. Newman, J.R. Lanzante, N.-C. Lau, and J.D. Scott, 2002: The atmospheric bridge: The influence of ENSO teleconnections on air-sea interaction over the global oceans. *J. Climate*, submitted.

Carton, J.A., G. Chepurin, and X. Cao, 2000: A simple ocean data assimilation analysis of the global upper ocean 1950–95. Part I: Methodology. *J. Phys. Oceanogr.*, **30**, 311–326.

Cayan, D.R., 1992: Latent and sensible heat flux anomalies over the northern oceans: Driving the sea surface temperature. *J. Phys. Oceanogr.*, **22**, 859–881.

Deser, C., M.A. Alexander, and M.S. Timlin, 1996: Upper-ocean thermal variations in the North Pacific during 1970–1991. *J. Climate*, **9**, 1840–1855.

———, ———, and ———, 1999: Evidence for a wind-driven intensification of the Kuroshio Current Extension from the 1970s to the 1980s. *J. Climate*, **12**, 1697–1706.

Fraedrich, K., C. Ziehmann, and F. Sielmann, 1995: Estimates of spatial degrees of freedom. *J. Climate*, **8**, 361–369.

Frankignoul, C., 1985: Sea surface temperature anomalies, planetary waves, and air-sea feedback in the middle latitudes. *Rev. Geophys.*, **23**, 357–390.

Giese, B.S. and J.A. Carton, 1999: Interannual and decadal variability in the tropical and midlatitude Pacific Ocean. *J. Climate*, **12**, 3402–3418.

Haney, R.L., 1971: Surface thermal boundary conditions for ocean general circulation models. *J. Phys. Oceanogr.*, **1**, 241–248.

Huang, R.X. and B. Qiu, 1994: Three-dimensional structure of the wind-driven circulation in the subtropical North Pacific. *J. Phys. Oceangr.*, **24**, 1608–1622.

Kalnay, E.M. et al., 1996: The NCEP/NCAR 40-year reanalysis project. *Bull. Amer. Meteor. Soc.*, **77**, 437–471.

Latif, M. and T.P. Barnett, 1994: Causes of decadal climate variability over the North Pacific and North America. *Science*, **266**, 634–637.

Miller, A.J., D.R. Cayan, T.P. Barnett, N.E. Graham, and J.M. Oberhuber, 1994: Interdecadal variability of the Pacific Ocean: model response to observed heat flux and wind stress anomalies. *Clim. Dyn.*, **9**, 287–302.

———, ———, and W.B. White, 1998: A westward-intensified decadal change in the North Pacific thermocline and gyre-scale circulation. *J. Climate*, **11**, 3112–3127.

Nakamura, H., G. Lin, and T. Yamagata, 1997: Decadal climate variability in the North Pacific during the recent decades. *Bull. Amer. Meteor. Soc.*, **78**, 2215–2225.

Parker, D.E., C.K. Folland, and M. Jackson, 1995: Marine surface temperature: Observed variations and data requirements. *Clim. Change*, **31**, 559–600.

Peng, S., W.A. Robinson, and M.P. Hoerling, 1997: The modeled atmospheric response to mid latitude SST anomalies and its dependence on background circulation states. *J. Climate*, **10**, 971–987.

Qiu, B. and K.A. Kelly, 1993: Upper-ocean heat balance in the Kuroshio Extension region. *J. Phys. Oceanogr.*, **23**, 2027–2041.

———, 2000: Interannual variability of the Kuroshio Extension system and its impact on the wintertime SST field. *J. Phys. Oceanogr.*, **30**, 1486–1502.

Rayner, N.A., E.B. Horton, D.E. Parker, C.K. Folland, and R.B. Hackett, 1996: Version 2.2 of the global sea-ice and sea surface temperature data set, 1903–1994. *Climate Research Technical Note*, **74**, 1–21.

Schneider, N., A.J. Miller, and D.W. Pierce, 2002: Anatomy of North Pacific decadal variability. *J. Climate*, **15**, 586–605.

Seager, S., Y. Kushnir, N.H. Naik, M.A. Cane, and J. Miller, 2001: Wind-driven shifts in the latitude of the Kuroshio–Oyashio Extension and generation of SST anomalies on decadal timescales. *J. Climate*, **14**, 4249–4265.

Tanimoto, Y., N. Iwasaka, K. Hanawa, and Y. Toba, 1993: Characteristic variations of sea surface temperature with multiple time scales in the North Pacific. *J. Climate*, **6**, 1153–1160.

Tomita, T., B. Wang, T. Yasunari, and H. Nakamura, 2001: Global patterns of decadal scale variability observed in sea surface temperature and lower-tropospheric circulation fields. *J. Geophys. Res.*, **106**, 26805–26815.

Xie, S.-P., Y. Tanimoto, H. Noguchi, and T. Matsuno, 1999: How and why climate variability differs between the tropical Pacific and Atlantic. *Geophys. Res. Lett.*, **26**, 1609–1612.

———, T. Kunitani, A. Kubokawa, M. Nonaka, and S. Hosoda, 2000: Interdecadal thermocline variability in the North Pacific for 1958–97: A GCM simulation. *J. Phys. Oceanogr.*, **30**, 2798–2813.

Yulaeva, E., N. Schneider, D.W. Pierce, and T.P. Barnett, 2001: Modeling of North Pacific climate variability forced by oceanic heat flux anomalies. *J. Climate*, **14**, 4027–4046.

Yasuda, I., T. Tozuka, M. Noto, and S. Kouketsu, 2000: Heat balance and regime shifts of the mixed layer in the Kuroshio Extension. *Prog. Oceanogr.*, **47**, 257–278.

Yasuda, T. and K. Hanawa, 1997: Decadal changes in the mode waters in the midlatitude North Pacific. *J. Phys. Oceanogr.*, **27**, 858–870.